Ab initio ground potential energy surface ($^3A''$) for the $O(^3P)+N_2O$ reaction and kinetics study

Miguel González,[a] Rosendo Valero, and R. Sayós[a]
Departament de Química Física i Centre de Recerca en Química Teòrica, Universitat de Barcelona, C/ Martí i Franquès, 1. 08028 Barcelona, Spain

(Received 30 January 2001; accepted 2 May 2001)

An *ab initio* CASPT2//CASSCF study of the $^3A''$ ground potential energy surface for the $O(^3P)+N_2O(X\,^1\Sigma^+)$ reaction has been performed, investigating the two predominant reactive channels. Symmetry breaking is reported for some of the structures. Rate constants are calculated by means of the transition state theory yielding values in almost quantitative agreement with experiment for the 2 $NO(X\,^2\Pi)$ channel, but at variance with experiment for the $N_2(X\,^1\Sigma_g^+)+O_2(X\,^3\Sigma_g^-)$ one. A preliminary study on the possible existence of surface crossings ($^3A''-{}^1A'$, $^3A''-{}^1A''$, and $^3A''-{}^3A'$ intersections) reveals that more efforts are warranted to fully explain the origin of this discrepancy.
 [DOI: 10.1063/1.1381010]

I. INTRODUCTION

The N_2O molecule plays a relevant role in combustion processes as a generator of NO_x species. Also, its thermal decomposition leads to oxygen atoms in their first singlet excited state, which participate in the stratospheric ozone cycle. In combustion processes, the reaction of the nitrous oxide molecule with ground state $O(^3P)$ atoms is of major importance. The $O(^3P)+N_2O$ reaction presents two product channels:

$$O(^3P)+N_2O(X\,^1\Sigma^+)\rightarrow NO(X\,^2\Pi)+NO(X\,^2\Pi),$$

$$\Delta H^0_{0\ K}=-36.0\ \text{kcal mol}^{-1} \qquad (1)$$

$$\rightarrow N_2(X\,^1\Sigma_g^+)+O_2(X\,^3\Sigma_g^-),$$

$$\Delta H^0_{0\ K}=-79.6\ \text{kcal mol}^{-1}. \qquad (2)$$

Under C_s symmetry one $^3A'$ and two $^3A''$ potential energy surfaces (PESs) correlate with the products of channel (1) while only one $^3A''$ PES correlates with the products of channel (2). Thus, in C_s symmetry both reactions are feasible only through the ground PES ($^3A''$).

Many experimental studies have been devoted to the determination of the rate constants for reactions (1) and (2).[1] However, it was not until very recently that direct measurements of the total rate constant at an intermediate temperature range were performed.[2] Later, a critical assessment of all the available information was carried out.[1] From the selected works, the expression $k_1=1.52\times10^{-10}\exp(-13\,930/T)$ (1370–4080 K) $\text{cm}^3\,\text{molecule}^{-1}\,\text{s}^{-1}$ was derived for reaction (1). Analogously, for reaction (2) the expression $k_2=6.13\times10^{-12}\exp(-8020/T)$ (1075–3340 K) $\text{cm}^3\,\text{molecule}^{-1}\,\text{s}^{-1}$ was finally obtained. Thus, activation energies of 27.7 and 15.9 kcal mol^{-1} are deduced for reactions (1) and (2), respectively.

On the other hand, to our knowledge no theoretical studies of the system exist, apart from a quotation in Ref. 1 of an unpublished *ab initio* study yielding a barrier height for reaction (1) of 28 kcal mol^{-1}, in good accordance with experiment, and a much higher barrier for reaction (2) at variance with the results of Ref. 1. In the latter case, a crossing of the $^3A''$ surface with the ground singlet surface ($^1A'$) of the $O(^1D)+N_2O$ system is suggested as a lower-energy alternative pathway to products, N_2+O_2.

II. METHODOLOGY

In the study of a PES, it is important to introduce all the configurations that have an important weight in one or another of its regions. In this way, a balanced description of, e.g., reactants and products, transition states, avoided crossings, etc., should in principle be achieved. In the CASSCF (complete active space self-consistent-field) method[3] all the configuration state functions (CSFs) generated from a fixed set of molecular orbitals (MOs), called the active space, are included. This method is intended to account for most of the nondynamical electronic correlation. As such, it is not expected to yield reliable relative energies within the PES. Therefore, the dynamical correlation must also be accounted for. To this aim, we have chosen the CASPT2 approach[4,5] in which the CASSCF wave function is taken as the zeroth-order function to calculate the energy at the second order of perturbation theory. This method has been employed with great success in the prediction of geometries and binding energies[6] as well as in the calculation of electronic spectra of small to medium-sized molecules.[7] In this work we have adopted the CASPT2//CASSCF methodology, that is, optimal geometries are obtained at the CASSCF level and CASPT2 pointwise calculations are performed on the resulting structures. The CASPT2//CASSCF method has an esti-

[a]Authors to whom correspondence should be addressed. Electronic mail: miguel@qf.ub.es and r.sayos@qf.ub.es

mated error in exoergicities of ± 2 kcal mol^{-1}, provided all the valence electrons are active and a large enough basis set is employed.

In practice, the most important aspect of the CASSCF method is the election of the active space, to which different approaches can be found in the literature.[8,9] In general, the selected MOs must be such that their corresponding natural orbital occupation numbers (NOONs) are within the range 0.02–1.98, so as to account for the nondynamical correlation only. Also, it has been shown that to obtain the lowest energy for a given size of the active space the NOONs must be as different as possible from two or zero,[8] and that the active space should be homogeneous throughout the PES so as to avoid discontinuities. However, the lowest energy and homogeneity criteria are not easy to fulfil simultaneously for all nuclear configurations.[10] The problem is more acute the smaller the active space is. These considerations are important for the present study, as it will be shown below.

In reactants $[O(^3P)+N_2O]$, the dominant configuration presents two triplet-coupled electrons in two $2p$ atomic oxygen orbitals, leaving the third $2p$ orbital doubly occupied. A reasonable election is to take the MOs generated from all the $2p$ atomic orbitals of the N_2O_2 system as the active space, i.e., a 14-electrons-in-12-orbitals or (14,12) active space. However, it leads to an NOON of two for the atomic oxygen orbital carrying two paired electrons. Thus, it should not be taken as active according to the 0.02–1.98 criterion. Further, the energy drops considerably on substituting this orbital for one of the $2s$-derived MOs in the N_2O molecule, which presents a NOON of about 1.98. This situation was found not only in reactants but also all along the entrance region of the PES. To the contrary, for the intermediate and exit regions of channel (1) and for the exit region of channel (2) all the $2p$-derived MOs are required, as all have NOONs essentially between 1.98 and 0.02. For channel (1) this fact generates an important energy gap between the entrance region and the other regions, so that the transition states (TSs) in the entrance region are lower in energy than the minima in the intermediate region. On the other hand, if the $2s$-derived MO is kept in the intermediate region of channel (1) the CASSCF wave function is not well balanced, leading incorrectly to unsymmetrical stationary points. Following parallel work we are performing on the $O(^1D)+N_2O$ reaction, we added two more $2s$-derived MOs to the active space to yield an 18-electrons-in-14-orbitals or (18,14) active space. Again, one has two (18,14) active spaces, one in which three $2s$-derived MOs are present (reactants and entrance region, *A*-type space) and one with two $2s$-derived MOs and all the $2p$-derived ones (rest of channel (1) and N_2+O_2, *B*-type space). In this manner, the TSs turn out to be placed above the minima to which they lead. In the reactants region, the *A*-type active space is the only one that can be made to converge; all attempts to obtain a *B*-type active space in this region were unsuccessful.

In this work we have employed the (14,12) active space in the search and characterization of the stationary points on the $^3A''$ PES by means of CASSCF analytical gradients. These stationary points were then reoptimized with the (18,14) active space. The CASSCF (18,14) calculations amount to about 900 000 CSFs in C_s symmetry. Eventually, the active space has been reduced so as to carry out studies on surface crossing (see below). Numerical characterization was needed for some of the structures (see below). To this aim, the SURVIBTM program of rovibrational analysis was employed.[11] Pointwise CASPT2 calculations with both active spaces were performed on all the structures. The standard Cartesian Gaussian 6-31G(d) (Ref. 12) and 6-311G($2d$) (Refs. 13 and 14) basis sets of Pople and coworkers were selected. This basis set of triple-zeta quality plus two sets of polarization basis functions allowed us to achieve a rather correct description of the $N(^2D)+NO(X\,^2\Pi)$ reaction[15] as well as of the highly demanding van der Waals $(NO)_2$ dimers[16] in previous works of our own, in which the CASPT2 and CASPT2//CASSCF methods were employed, respectively. All the stationary points were characterized as either minima (MIN) or transition states by numerical calculation of their CASSCF harmonic vibrational frequencies. The G2 variant of the CASPT2 method was selected.[17] In hereafter, the acronym CASPT2 will stand for the CASPT2 G2 method. The calculations were performed by using the MOLCAS 4.1 (Ref. 18) and the GAUSSIAN 98 (Ref. 19) packages of electronic structure calculations.

III. RESULTS AND DISCUSSION

In Tables I, II, and III we show the geometries, harmonic vibrational frequencies and energies of the stationary points obtained, respectively. In Figs. 1 and 2 the energy profiles of channels (1) and (2), respectively, are presented.

As for the properties of reactants and products, the geometries optimized at the CASSCF level are quite accurate (Table I), although the bond distances are always slightly overestimated [0.6–1.1 % and average value of 0.6% for CASSCF(18,14)] with respect to experiment. The frequencies show a maximum deviation of 33 cm^{-1} (Table II) with the relative errors being in the interval 0.3–2.1 % for CASSCF(18,14) (average value of 1.1%). The exoergicities of reaction are also in good agreement with experiment (Table III), although the error for channel (1) [3.4 kcal mol^{-1} (9.3%) for CASPT2//CASSCF(18,14)] is slightly larger than the average estimated accuracy of the CASPT2 method.

A qualitative description of the $^3A''$ PES can be done in terms of the dominant electronic configurations, which are detailed in Table IV. It is remarkable that $O+N_2O$, MIN A1, TS A1, and 2 NO [channel (1)], as well as N_2+O_2 [channel (2)], present only one main CSF, with a CI coefficient higher than 0.90. Note also that in MIN C1 and MIN D1 [channel (1), NO-dimers] and in TS B2 [channel (2)] the two dominant CSFs have almost an equal weight. As one can see in Fig. 1 [CASPT2//CASSCF(18,14) energy plus CASSCF(14,12) zero-point energy (ZPE)], in channel (1) the oxygen atom can follow either a *cis*- or a *trans*-approximation to the N_2O molecule passing through the shallow van der Waals structure MIN A1. This structure is common to both channels, as the oxygen atom is closer to the N central atom in the N_2O molecule. A slight distortion either to the terminal N atom or to the oxygen atom leads to channels (1) or (2), respectively. The barrier height including ZPE, though 5.7 kcal mol^{-1} smaller for the *cis*-approx-

TABLE I. Geometries of the stationary points on the $^3A''$ PES at the CASSCF(18,14) level.[a]

Reactants and products	$R_{NN'}$/Å	$R_{N'O'}$/Å	$R_{OO'}$/Å	<NN′O′/°	<N′O′O/°	Dihedral/°
$O(^3P)+N_2O$[c]	1.1343	1.1931		180.0		
	(1.1323)	(1.1901)		(180.0)		
	[1.1273]	[1.1851]		[180.0]		
NO+NO[d]		1.1605				
		(1.1586)				
		[1.1508]				
$N_2+O_2(X\,^3\Sigma_g^-)$[d]	1.1045		1.2207			
	(1.1037)		(1.2197)			
	[1.0977]		[1.2075]			
Reaction channel (1)	$R_{NN'}$/Å	$R_{N'O'}$/Å		<NN′O′/°,<ONN′/°		Dihedral/°[b]
MIN A1	1.1339	1.1931,3.5925		179.9,65.2		180.0
	(1.1320)	(1.1900,3.5926)		(179.9,65.1)		(180.0)
TS A1	1.2140	1.2011,1.6059		148.2,108.4		0.0
	(1.2175)	(1.1983,1.6085)		(146.9,107.5)		(0.0)
MIN B1 ($^3A_2$)	1.2822	1.3043,13043		113.0,113.0		0.0
	(1.3243)	(1.3000,1.3000)		(108.6,108.6)		(0.0)
TS B1[e]	(1.3578)	(1.2960,1.2971)		(108.7,110.9)		(0.0)
MIN C1 ($^3B_1$)	3.6767	1.1632,1.1632		84.3,84.3		0.0
	(3.6794)	(1.1628,1.1628)		(84.0,84.0)		(0.0)
TS D1	1.2094	1.2040,1.6530		146.8,105.7		180.0
	(1.2124)	(1.2025,1.6555)		(146.0,104.1)		(180.0)
MIN D1 (^3A_u)	3.4547	1.1634,1.1634		108.7,108.7		180.0
	(3.4927)	(1.1624,1.1624)		(105.9,105.9)		(180.0)
Reaction channel (2)	$R_{NN'}$/Å	$R_{N'O'}$/Å	$R_{OO'}$/Å	<NN′O/°	<OO′N′/°	Dihedral/°[b]
MIN A1	1.1339	1.1931	3.3650	179.9	75.9	0.0
	(1.1320)	(1.1900)	(3.3650)	(179.9)	(75.8)	(0.0)
TS A2	1.1483	1.3942	1.6620	138.9	115.6	0.0
	(1.1527)	(1.3715)	(1.6518)	(137.8)	(114.6)	(0.0)
TS B2[f]	(1.1618)	(1.4025)	(1.8072)	(130.5)	(100.4)	(180.0)

[a]The CASSCF(14,12) geometries are shown in parentheses. The available experimental data are given in brackets.
[b]The connectivity of the atoms is assumed to be O–N–N′–O′ for channel (1) and N–N′–O′–O for channel (2), where O is the attacking O atom. Hence, in each case the dihedral angle is given according to this connectivity. Only the relevant bonding parameters for each structure are reported.
[c]Experimental data taken from Ref. 20.
[d]Experimental data taken from Ref. 21.
[e]Derived from an analytical fit of 60 C_{2v}/C_s 50:50 average $^3A_2/^3B_1$ ($1/2\,^3A''$) points located near an avoided crossing or a conical intersection of these states. A second order polynomial was employed obtaining a RMSD of 4.5×10^{-5} a.u. (3×10^{-2} kcal mol^{-1}).
[f]Derived from an analytical fit of 72 C_s/C_1 50:50 average $1/2\,^3A''$ ($1/2\,^3A$) points located near an avoided crossing or a conical intersection of these states. A second order polynomial was employed obtaining a RMSD of 1.8×10^{-5} a.u. (1×10^{-2} kcal mol^{-1}).

imation, is in both cases relatively large (24.1 and 29.8 kcal mol^{-1} for the *cis*- and *trans*-approaches, respectively). This fact can be justified if one considers that the $N_2O(X\,^1\Sigma^+)$ molecule is a closed-shell species in which an electronic promotion must take place prior to forming a bond with the open-shell oxygen atom. From TS A1 [*cis*-TS, C_s structure ($^3A''$)] the system can evolve to the more symmetric (C_{2v}) MIN B1 ($^3A_2$). However, TS D1 [*trans*-TS, C_s structure ($^3A''$)] can connect directly with MIN D1 [C_{2h} structure (^3A_u), NO-dimer *trans*-structure], and from this stationary point it can reach products. On elongation of the NN bond in MIN B1, an avoided crossing or a conical intersection between the ground and the first excited $^3A''$ PES derived from $O(^3P)+N_2O$ is patent, their CASSCF energies being very close to each other. As in the region near MIN B1 (C_{2v} symmetry) the excited $^3A''$ state belongs to the $^3B_1$ irreducible representation, it cannot interact with the ground state, which is classified as $^3A_2$. On distortion of the system to C_s symmetry, both states mix with each other because they belong to the same irreducible representation. Besides, a nearby transition state [TS B1, C_s structure ($^3A''$)] is located on the lowest PES. Numerical characterization was needed to obtain the structure and frequencies of TS B1, since single-root CASSCF gives rise to a cusp behavior (i.e., the energy is not a smooth function of the nuclear coordinates). Another, previously reported example of this kind of behavior is the weakly avoided crossing between the neutral and the ionic states of the LiF system.[24] In both cases, discontinuities in the wave function arise at points close to the crossing, where the wave function should switch smoothly from one dominant configuration to the other. This phenomenon can be explained by the poor description of anyone configuration in terms of the MOs optimized in a situation where the other one is dominant. Furthermore, in the LiF system MRCI calculations on single-root CASSCF wave functions, although intended to remedy the deficiencies of the latter, lead to sharp discontinuities in the dipole moment function. The only way around this problem seems to be to introduce a state-average CASSCF wave function, as we have also done, with the inconvenient that no analytical gradients were available to us

TABLE II. Harmonic vibrational frequencies (in cm^{-1}) of the $^3A''$ stationary points at the CASSCF(14,12) level.[a]

Stationary point	ν_1	ν_2	ν_3	ν_4	ν_5	ν_6
$O(^3P)+N_2O$[b]	2315.1(σ^+) [2282.1]	1317.6(σ^+) [1298.3]	593.0(π) [596.3]			
NO+NO[c]	1915.1(σ^+) [1904.2]					
$N_2+O_2(X\ ^3\Sigma_g^-)$[c]	2365.9(σ_g^+)(N_2) [2358.6]	1547.1(σ_g^+)(O_2) [1580.2]				
			Reaction channel (1)			
MIN A1	2274.4 (a')	1296.9 (a')	604.0 (a')	601.9 (a'')	62.8 (a')	38.8 (a')
TS A1	893.6i (a')	1759.5 (a')	1178.5 (a')	700.8 (a')	553.8 (a'')	269.2 (a')
MIN B1 ($^3A_2$)	1161.4 (a_1)	1115.0 (a_1)	1001.8 (b_2)	863.5 (b_2)	546.0 (a_2)	429.0 (a_1)
TS B1[d]	1850.7i (a')	2376.2 (a')	1131.0 (a')	825.0 (a')	449.6 (a')	(a'')
MIN C1 ($^3B_1$)[c]						
TS D1	984.0i (a')	1744.4 (a')	1117.2 (a')	669.2 (a')	411.0 (a')	312.8 (a')
MIN D1 (^3A_u)[e]						
			Reaction channel (2)			
MIN A1	2274.4 (a')	1296.9 (a')	604.0 (a')	601.9 (a'')	62.8 (a')	38.8 (a')
TS A2	1320.3i (a')	1792.9 (a')	662.8 (a')	500.8 (a')	375.9 (a'')	188.5 (a')
TS B2[f]	1969.2i (a')	1497.9 (a')	571.8 (a')	430.2 (a')	278.8 (a')	204.8 (a'')

[a]The symmetries of the normal vibrational modes are given in parentheses, and the available experimental data are given in brackets. The modes are ordered from larger to smaller frequencies.
[b]Experimental data taken from Ref. 20.
[c]Experimental data taken from Ref. 21.
[d]Frequencies from analytical fit (see Table I). The out-of-plane frequency could not be calculated because of numerical problems (see text).
[e]Frequencies of the dimers not calculated because of the symmetry-breaking problem.
[f]Frequencies from analytical fit (see Table I).

for this kind of calculation. The energies for TS B1 in Table III are reported at the state-average level with the two states equally weighted. An estimate of the error committed with respect to the single-root energy can be made by calculating both energies at the closer stationary point, MIN B1. The obtained difference is slightly below 2 kcal mol^{-1} at both the CASSCF and the CASPT2 levels. The relevant CSFs and their CI coefficients for the lowest $^3A''$ state in TS B1 are

TABLE III. Energies of the $^3A''$ PES stationary points calculated at different levels.[a,b]

Stationary point	CASSCF(14,12)	CASPT2//CASSCF(14,12)	CASSCF(18,14)	CASPT2//CASSCF(18,14)	Experiment[c]
$O(^3P)+N_2O$	0.0 (0.0)	0.0 (0.0)	0.0 (0.0)	0.0 (0.0)	0.0 (0.0)
NO+NO	−26.0 (−24.6)	−32.4 (−31.0)	−28.2 (−26.8)	−33.3 (−31.9)	−36.7 (−35.3)
$N_2+O_2(X\ ^3\Sigma_g^-)$	−71.2 (−69.9)	−81.2 (−79.9)	−72.7 (−71.4)	−80.7 (−79.4)	−80.2 (−78.9)
		Reaction channel (1)			
MIN A1	−0.5 (−0.6)	−1.1 (−1.2)	−0.5 (−0.6)	−1.1 (−1.2)	
TS A1	50.5 (51.0)	23.7 (24.2)	48.9 (49.4)	24.1 (24.6)	
MIN B1 ($^3A_2$)	57.7 (57.3)	19.4 (19.0)	48.4 (48.0)	16.3 (15.9)	
TS B1[d]	58.9 (59.0)	15.9 (16.0)	45.8 (45.9)	15.1 (15.2)	
MIN C1 ($^3B_1$)[e]	−0.2 (−0.2)	−0.8 (−0.8)	−0.2 (−0.2)	−0.8 (−0.8)	
TS D1	57.1 (57.9)	29.4 (30.2)	54.3 (55.1)	29.8 (30.6)	
MIN D1 (^3A_u)[e]	−0.3 (−0.3)	−0.8 (−0.8)	−0.3 (−0.3)	−0.8 (−0.8)	
		Reaction channel (2)			
MIN A1	−0.5 (−0.6)	−1.1 (−1.2)	−0.5 (−0.6)	−1.1 (−1.2)	
TS A2	61.3 (63.1)	38.4 (40.3)	59.2 (61.0)	38.5 (40.3)	
TS B2[d]	77.6 (80.2)	55.8 (58.4)	75.6 (78.2)	56.3 (58.9)	

[a]Energies are given in kcal mol^{-1} with respect to reactants. For MIN C1 and MIN D1, it is more convenient to give them relative to products. The absolute energies of reactants at each one of the levels considered are as follows: CASSCF(14,12), −258.744 475 a.u.; CASPT2//CASSCF(14,12), −259.337 241 a.u.; CASSCF(18,14), −258.752 660 a.u.; and CASPT2//CASSCF(18,14), −259.339 496 a.u.
[b]Energies with (without) ZPE without (in) parentheses.
[c]Data derived from Refs. 20–23.
[d]Pointwise state-average calculations on the geometry obtained by means of an analytical fit (see Table I).
[e]ZPEs derive from frequencies assumed to be equal to those of 2 NO molecules (see Table II).

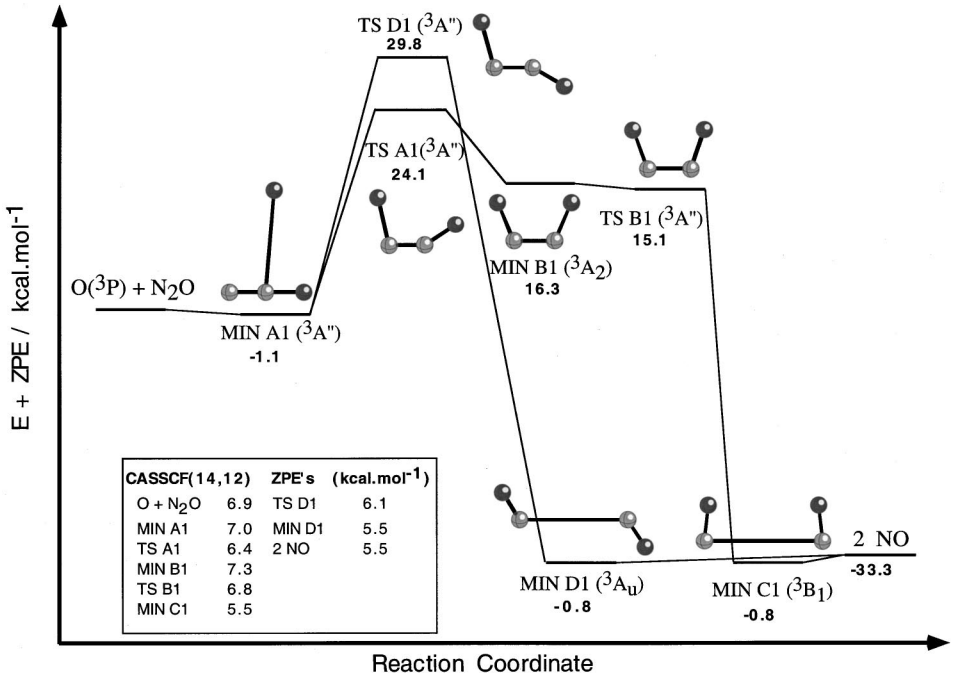

FIG. 1. Schematic representation of the structures of the stationary points for channel (1) obtained at the CASSCF(18,14) level including energies [CASPT2//CASSCF(18,14) plus CASSCF(14,12) ZPE] relative to reactants [$O(^3P)+N_2O$] except for MIN C1 and MIN D1, which are given relative to products (2 NO). For TS B1, the MIN B1 out-of-plane frequency was assumed to calculate the ZPE (see Table II).

given in Table IV. These coefficients are interchanged in the second $^3A''$ state. Proceeding further along the reaction path, the wave function acquires an increasing $^3B_1$ character, leading finally to MIN C1, NO-dimer *cis*-structure, and products (2 NO).

In channel (2) [see Fig. 2 (CASPT2//CASSCF(18,14) energy plus CASSCF(14,12) ZPE], similar structures are found in the entrance region, i.e., apart from the weakly bound MIN A1 [C_s structure ($^3A''$)], two TSs of *cis*-(TS A2) and *trans*-(TS B2) geometry [C_s structures ($^3A''$)] are characterized. The corresponding barrier heights are considerably higher than those in channel (1). Besides, TS B2 is about 18 kcal mol^{-1} above TS A2, while in channel (1) the already reported energy gap is only 5.7 kcal mol^{-1}. The larger instability of these structures could be justified by the weaker OO bond formed, which would compensate for a smaller portion of the required N_2O promotion energy. An avoided crossing or a conical intersection was also evident near TS B2, for which the same comments as for TS B1 regarding the need of using a state-average wave function can be applied. Note that the second $^3A''$ state correlates with products in an excited state, while in TS B1 both the ground and first excited states correlate with products in their ground state. As one can notice from Table IV, the two main CSFs have almost equal CI coefficients in TS B2, which would indicate the proximity to a crossing point. By analogy with the structures

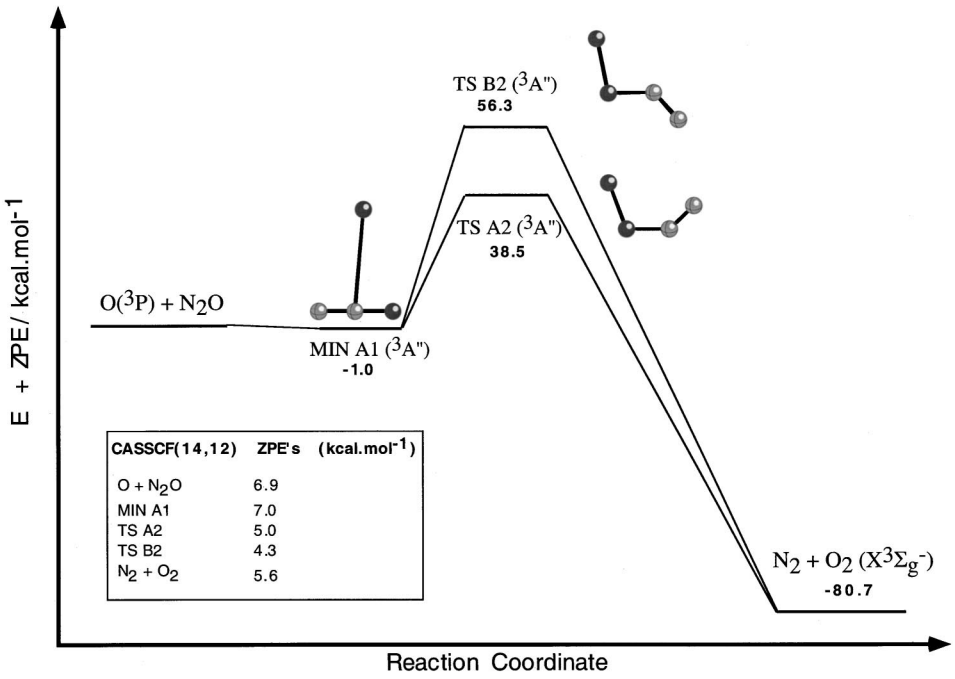

FIG. 2. Schematic representation of the structures of the stationary points for channel (2) obtained at the CASSCF(18,14) level including energies [CASPT2//CASSCF(18,14) plus CASSCF(14,12) ZPE] relative to reactants [$O(^3P)+N_2O$].

TABLE IV. Electronic configurations and active spaces of the $^3A''$ stationary points at the CASSCF(18,14) level.

Reaction channel (1)		Inactive	Active	Electronic configurations[a]
$O+N_2O$	(C_s)	$6a'$	$10a'+4a''$	$[12a'^2\,2a''^2]1a'^1\,1a''^1$ (0.94)
MIN A1	(C_s)	$6a'$	$10a'+4a''$	$[12a'^2\,2a''^2]1a'^1\,1a''^1$ (0.94)
TS A1	(C_s)	$6a'$	$10a'+4a''$	$[12a'^2\,2a''^2]1a'^1\,1a''^1$ (0.91)
MIN B1 ($^3A_2$)	(C_{2v})	$3a_1+3b_2(6a')$	$5a_1+5b_2+2a_2+2b_1(10a'+4a'')$	$[7a_1^2\,5b_2^2\,1a_2^2\,1b_2^2]1b_2^1\,1b_1^1/[6a_1^2\,6b_2^2\,2b_1^2]1a_1^1\,1a_2^1$ (0.86/0.25)
TS B1	(C_s)	$6a'$	$10a'+4a''$	$11a'^2\,1a'^1\,1a'^2\,2a''^2\,1a''^1/11a'^2\,1a'^2\,1a'^1\,2a''^2\,1a''^1$ (0.84/0.10)[b]
MIN C1 ($^3B_1$)	(C_{2v})	$3a_1+3b_2(6a')$	$5a_1+5b_2+2a_2+2b_1(10a'+4a'')$	$[6a_1^2\,6b_2^2\,1a_2^2\,1b_2^2]1a_1^1\,1b_1^1/[6a_1^2\,6b_2^2\,1a_2^2\,1b_1^2]1b_2^1\,1a_2^1$ (0.67/0.64)
TS D1	(C_s)	$6a'$	$10a'+4a''$	$[12a'^2\,2a''^2]1a'^1\,1a''^1$ (0.90)
MIN D1 (^3A_u)	(C_{2h})	$3a_g+3b_u(6a')$	$5a_g+2b_g+2a_u+5b_u(10a'+4a'')$	$[6a_g^2\,1b_g^2\,1a_u^2\,6b_u^2]1a_g^1\,1a_u^1/[6a_g^2\,1b_g^2\,1a_u^2\,6b_u^2]1b_g^1\,1b_u^1$ (0.68/−0.64)
2 NO	(C_s)	$6a'$	$10a'+4a''$	$[12a'^2\,2a''^2]1a'^1\,1a''^1$ (0.94)
Reaction channel (2)				
$O+N_2O$	(C_s)	$6a'$	$10a'+4a''$	$[12a'^2\,2a''^2]1a'^1\,1a''^1$ (0.94)
MIN A1	(C_s)	$6a'$	$10a'+4a''$	$[12a'^2\,2a''^2]1a'^1\,1a''^1$ (0.94)
TS A2	(C_s)	$6a'$	$10a'+4a''$	$[12a'^2\,2a''^2]1a'^1\,1a''^1$ (0.89)
TS B2	(C_s)	$6a'$	$10a'+4a''$	$12a'^2\,1a'^1\,1a'^0\,2a''^2\,1a''^1/12a'^2\,1a'^0\,1a'^1\,2a''^2\,1a''^1$ (0.59/0.58)[b]
$N_2+O_2(X\,^3\Sigma_g^-)$	(C_s)	$6a'$	$10a'+4a''$	$[12a'^2\,2a''^2]1a'^1\,1a''^1$ (0.93)

[a]Leading configurations and CI coefficients for each stationary point are given. For the configurations, the number of orbitals belonging to each irreducible representation is indicated. The doubly occupied orbitals are enclosed in brackets while the singly occupied ones are given in the last place.
[b]The orbitals which change their occupancies between the two crossing configurations are explicitly indicated.

reported in channel (1), two van der Waals minima of *cis*- and *trans*-geometries in the exit valley are expected, although they are not shown in Fig. 2. However, as no such minima have been reported experimentally, we did not try to locate these presumably very shallow structures.

In Table I we note the important quantitative differences that exist between the CASSCF (14,12) and (18,14) geometries of MIN B1, while they are very similar for the other stationary points. These discrepancies are due to the important $2s$-derived active MOs lacking in the (14,12) space, whose NOONs are 1.99 and 1.98, indicating that they introduce a strong nondynamical correlation. For TS B1, the NOONs for these MOs are about the same as for MIN B1, so a geometry shift should also be expected. Unfortunately, in this case a pointwise characterization at the CASSCF(18,14) level was deemed too expensive to be carried out. We should mention that a certain difference in the NN distance and the NNO angle between the CASSCF(14,12) and (18,14) levels can also be noted in MIN D1. However, in this case the discrepancies can be attributed to the flatness of the PES rather than to an intrinsic better description at the CASSCF(18,14) level.

In Table II the harmonic vibrational frequencies are presented. They have been calculated only at the CASSCF(14,12) level because the CASSCF(18,14) calculations are computationally too expensive. For TS B1, the out-of-plane frequency could not be calculated because this coordinate is too flat to be numerically fitted. Also, problems with the CASSCF wave function were found for the $(NO)_2$ dimers (see below), so that for them the frequencies of products are assumed to evaluate the ZPE.

The energies of the stationary points are shown in Table III (see also Figs. 1 and 2). On moving from the CASSCF to the CASPT2 method there is a general stabilization of the stationary points, by about 30 kcal mol^{-1} in channel (1) and 20 kcal mol^{-1} in channel (2) with respect to reactants. In particular, a marked decrease in the barrier heights is apparent. It is worth mentioning that partial optimization of the triplet $(NO)_2$ dimers, MIN C1 (*cis*-) and MIN D1 (*trans*-) was performed in our previous work[16] at the CASPT2//CASSCF (18,14) level. Thus, the NO distance and NNO angle of the corresponding singlet dimers were assumed and energies for different values of the NN distance were fitted to a suitable polynomial expression. The resulting geometries and dissociation energies with and without the basis-set superposition error (BSSE) included were $R_{NN}=2.9885\,(3.2920)$ Å, $R_{NO}=1.1594$ Å, $<\mathrm{NNO}=94.5°$, $D_e=1.08(0.28)$ kcal mol^{-1} for MIN C1; and $R_{NN}=2.9764(3.1636)$ Å, $R_{NO}=1.1594$ Å, $<\mathrm{NNO}=109.1°$, $D_e=1.02(0.35)$ kcal mol^{-1} for MIN D1. The parameters including the BSSE are put in parentheses. It is patent the influence of the dynamical correlation in the shortening of the NN distances, as can be seen on comparing with Table I. Also, the BSSE has a great influence both on the NN distance and on the dissociation energy (D_e) in these van der Waals dimers.

Problems with the symmetry of the CASSCF wave function were present in MIN B1, in the region near TS B1 and in the $(NO)_2$ dimers. We reported on the same problem for the latter species in the work referred to above.[16] Briefly, when the molecular framework symmetry is not imposed on the CASSCF wave function, a lower-energy broken-symmetry solution is obtained. This phenomenon has been the subject of several theoretical studies. For a recent paper with many references see Ref. 25. Symmetry breaking is an example of the more general problem of instabilities in self-consistent-

field methods, like the single determinantal SCF method[26] and the CASSCF method.[27–28] We note that not even the state-average CASSCF method is completely free from this problem.[29] The broken symmetry orbitals are valence-bond-like, i.e., they are located in one atom or fragment rather than being spread over the whole molecule. In our case, localization of one electron in each one of the NO moieties in the $(NO)_2$ C_{2v}-symmetric structures is encountered. This effect becomes more acute on increasing the NN distance; thus, it does not take place in the entrance TSs. Whether symmetry breaking takes place or not depends on the balance between the so-called orbital size effect and resonance interactions.[30] Hence, the orbital sizes are optimal for localized electrons, while the delocalized solution can be regarded as a resonance between the localized solutions in which the orbitals are optimal only in an average way. For the above-mentioned $(NO)_2$ species, the resonance is not strong enough to prevent the electrons from localizing. The occurrence of this effect could be justified by the complicated electronic structure of MIN B1 and TS B1, in which two radical electrons are placed in different in- and out-of-plane MOs (see electronic configurations in Table IV), since it is known that open-shell species are particularly prone to symmetry breaking. For instance, several cases of broken symmetry are reported on open-shell C_{2v}-symmetric systems somewhat similar to the current triplet N_2O_2, like the doublet formyloxyl ($HCOO^{\cdot}$) radical,[30] the doublet and quartet states of the NO_2 molecule[31] or different triplet states of the CO_2 molecule.[32]

The spurious symmetry breaking must be distinguished from the real, physically motivated one, taking place in or near a conical intersection or an avoided crossing and caused by the nonadiabatic couplings, like that in TS B1.[33] To distinguish both types of effects, two calculations can be done at a symmetric structure, i.e., one in which the wave function keeps the molecular symmetry and another one in which it does not. If these energies differ from each other, as it happens for the above-mentioned structures, one faces a spurious symmetry breaking.

A different kind of broken symmetry was present in the $(NO)_2$ dimer region. In the 2 NO($X\,^2\Pi$) asymptote, if C_{2v} or C_{2h} symmetry is imposed on the CASSCF wave function, each of the NO fragments looked at separately keeps $C_{\infty v}$ symmetry with the radical electron distributed between the two degenerate π^* orbitals. However, if the symmetry is relaxed to C_s the electrons locate in only one orbital per NO molecule, thereby breaking the cylindrical symmetry. These two situations lead to an energy difference of several kcal mol^{-1}. Thus, even though the product calculation was performed in C_s symmetry (see Table IV), the dissociation energy of the dimers was calculated with respect to their same-symmetry C_{2v} or C_{2h} asymptotes. In this way, we are assuming that the C_s dissociation curve would be almost parallel to the C_{2v} or C_{2h} ones. In our work on the NO dimers we found this assumption to be a good compromise for this kind of symmetry breaking.[16]

To solve the firstly reported symmetry-breaking problem, we have employed the CAS SI (CAS–state interaction) method.[34,35] Application examples are available in the literature.[36,37] In this method, a nonorthogonal CI is applied to two broken-symmetry solutions, i.e., the one obtained in the actual calculation and that generated from it by means of application of the lacking molecular symmetry elements. Thus, for a symmetric structure (e.g., of C_{2v} symmetry) these solutions are mirror images of each other. The resulting CAS–SI MOs belong to the molecular symmetry point group, and can be given as input CASSCF orbitals. For C_s structures, that do not keep the molecular $(NO)_2$ mirror plane, the two solutions are no longer equivalent. Even in this case, CAS–SI is applied in the same way to yield delocalized solutions that join smoothly with the C_{2v} one.[25] We have found that by applying this method, the CASSCF wave function recovers the correct symmetry in the affected regions of the PES.

Finally, we have performed conventional transition state theory (TST)[38] rate constant calculations based on TS A1 and TS D1 [channel (1)] and TS A2 [channel (2)], as obtained at the CASPT2//CASSCF(18,14) level. We discarded TS B2, which would have a minor contribution to the rate constant. The level splitting owned to the spin–orbit interaction in O(^3P) has been taken account since it is expected to have an important effect on the electronic partition function for all but very high temperatures. Therefore, the rate constant for reaction (1) can be expressed as

$$k_{1,\mathrm{TST}} = \frac{3}{5+3e^{-E(^3P_1)/kT}+e^{-E(^3P_0)/kT}} \times (k(^3A'')+k(^3A')), \tag{3}$$

where $E(^3P_1)$ and $E(^3P_0)$ are, respectively, the energies of the $^3P_1$ and $^3P_0$ levels of O(^3P), 158.29 and 226.99 cm^{-1},[23] with respect to the lowest energy level ($^3P_2$). In this expression, $k(^3A'')$ and $k(^3A')$ derive from the classical expression of the TST rate constant excluding the electronic partition functions. In all transition state calculations, the rotational symmetry numbers are omitted. At this point we introduce the approximation that the contribution of the $^3A''$ and of the $^3A'$ PESs are equal, since our preliminary results on the $^3A'$ PES indicate strong similarity of their corresponding TS structures and energies. With this approximation, the following expression results:

$$k_{1,\mathrm{TST}} = \frac{6}{5+3e^{-E(^3P_1)/kT}+e^{-E(^3P_0)/kT}} \times [k(^3A'',\mathrm{TS\ A1})+k(^3A'',\mathrm{TS\ D1})]. \tag{4}$$

As for channel (2), since only the $^3A''$ PES correlates with reactants and products, one arrives at the expression:

$$k_{2,\mathrm{TST}} = \frac{3}{5+3e^{-E(^3P_1)/kT}+e^{-E(^3P_0)/kT}} [k(^3A'',\mathrm{TS\ A2})]. \tag{5}$$

Two levels of calculation have been considered: (a) simple TST level; (b) TST plus complete tunneling Wigner correction.[39] In the latter case the rate constant from a given TS takes the form

$$k_{\mathrm{TST(W)}} = \Gamma k_{\mathrm{TST}}, \tag{6}$$

TABLE V. Rate constants for the $O(^3P)+N_2O$ reaction.[a]

	Channel (1)			Channel (2)		
T/K	TST	TST (W)[b]	Experiment[c]	TST	TST (W)[b]	Experiment[d]
1000	1.26×10^{-16}	1.36×10^{-16}	1.36×10^{-16}	1.38×10^{-19}	1.60×10^{-19}	2.02×10^{-15}
1500	1.11×10^{-14}	1.15×10^{-14}	1.41×10^{-14}	1.49×10^{-16}	1.59×10^{-16}	2.92×10^{-14}
2000	1.19×10^{-13}	1.22×10^{-13}	1.44×10^{-13}	5.41×10^{-15}	5.63×10^{-15}	1.11×10^{-13}
2500	5.33×10^{-13}	5.41×10^{-13}	5.78×10^{-13}	4.96×10^{-14}	5.09×10^{-14}	2.48×10^{-13}
3000	1.51×10^{-12}	1.53×10^{-12}	1.46×10^{-12}	2.25×10^{-13}	2.29×10^{-13}	4.23×10^{-13}
3500	3.27×10^{-12}	3.30×10^{-12}	2.84×10^{-12}	6.81×10^{-13}	6.90×10^{-13}	6.20×10^{-13}
4000	5.98×10^{-12}	6.02×10^{-12}	4.67×10^{-12}	1.59×10^{-12}	1.61×10^{-12}	8.25×10^{-13}
4500	9.72×10^{-12}	9.76×10^{-12}	6.88×10^{-12}	3.12×10^{-12}	3.15×10^{-12}	1.03×10^{-12}
5000	1.45×10^{-11}	1.46×10^{-11}	9.37×10^{-12}	5.42×10^{-12}	5.46×10^{-12}	1.23×10^{-12}

[a]Rate constants are given in $cm^3\,molecule^{-1}\,s^{-1}$.
[b]In this case the complete Wigner tunneling correction has been applied to the TST calculations. See the text.
[c]Determined according to the expression: $k_1=1.52\times10^{-10}\exp(-13\,930/T)$ $cm^3\,molecule^{-1}\,s^{-1}$ (Ref. 1).
[d]Determined according to the expression: $k_2=6.13\times10^{-12}\exp(-8020/T)$ $cm^3\,molecule^{-1}\,s^{-1}$ (Ref. 1).

where Γ is the Wigner correction factor of the corresponding TS that is expressed as

$$\Gamma=1-\frac{1}{24}\left(\frac{h\nu_s}{kT}\right)^2\left(1+\frac{kT}{E_0}\right). \tag{7}$$

In this expression, ν_s is the imaginary frequency and E_0 is the barrier height (including the ZPE) for each one of the transition states considered.

The TST results for the temperature interval 1000–5000 K, which brackets the experimental range, are collected in Table V. Note the almost perfect agreement between the predicted rate constant values and the experiment for channel (1), as the Arrhenius plots in Fig. 3 make evident. This contrasts with the results for channel (2), in which different values for the classical barrier were considered, none of them giving even a reasonable agreement with experiment. To take deeper insight into this discrepancy, we have analyzed the possibility of a lower energy reaction path through an intersystem crossing (ISC). To do this, we have constructed a minimum energy path (MEP) between reactants and the lowest TS A1 by freezing the OO distance and optimizing the rest of geometric parameters at the CASSCF(14,12) level. The energies of the corresponding structures were calculated for the $^1A'$, $^1A''$, and $^3A''$ states. The results are shown in Fig. 4. In all points, a considerable energy gap between the triplet ground state and the singlet states is kept. Previously, an ISC for the $^3A''/^1A'$ PESs[40] was located. However, its

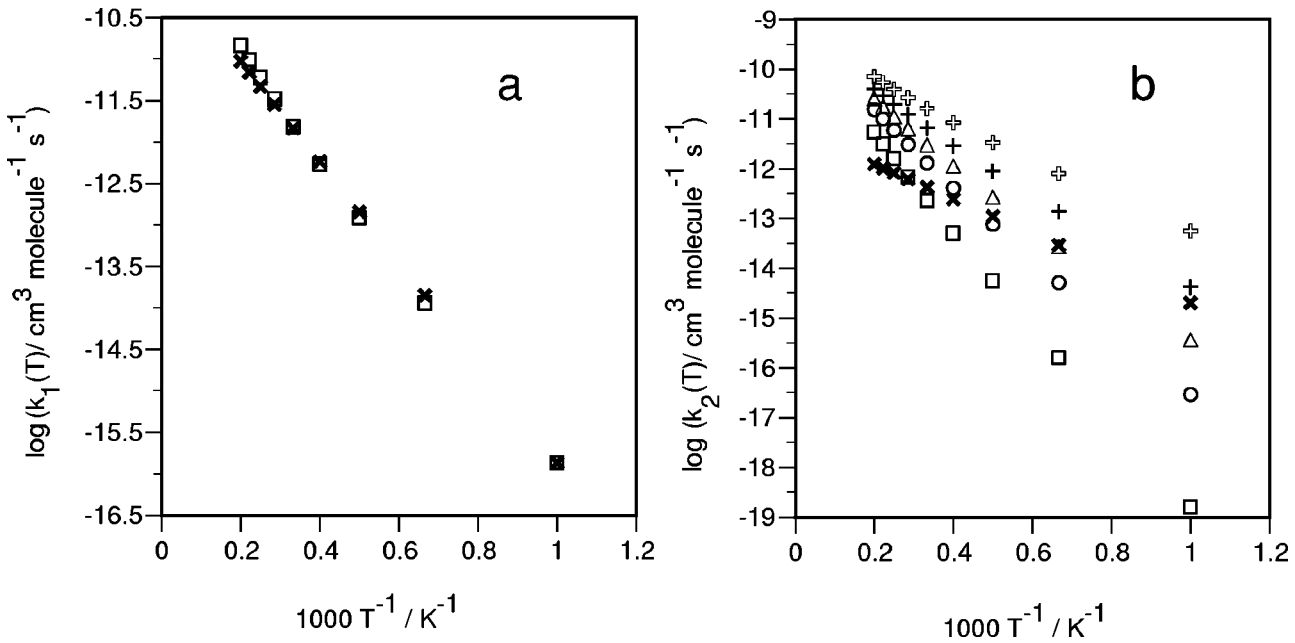

FIG. 3. Arrhenius plot of the rate constants for reactions (1) and (2) in the temperature interval 1000–5000 K. (a) Reaction (1): TST ("---□---"); experimental ("---×---") (Ref. 1). (b) Reaction (2) for which several values of the classical barrier height have been considered in the TST calculation: $E=40.3$ kcal mol^{-1} ("---□---"), $E=30.0$ kcal mol^{-1} ("---○---"), $E=25.0$ kcal mol^{-1} ("---△---"), $E=20.0$ kcal mol^{-1} ("---+---"), $\Delta E^{\neq}=15.0$ kcal mol^{-1} ("---open plus sign---"); experimental ("---×---") (Ref. 1).

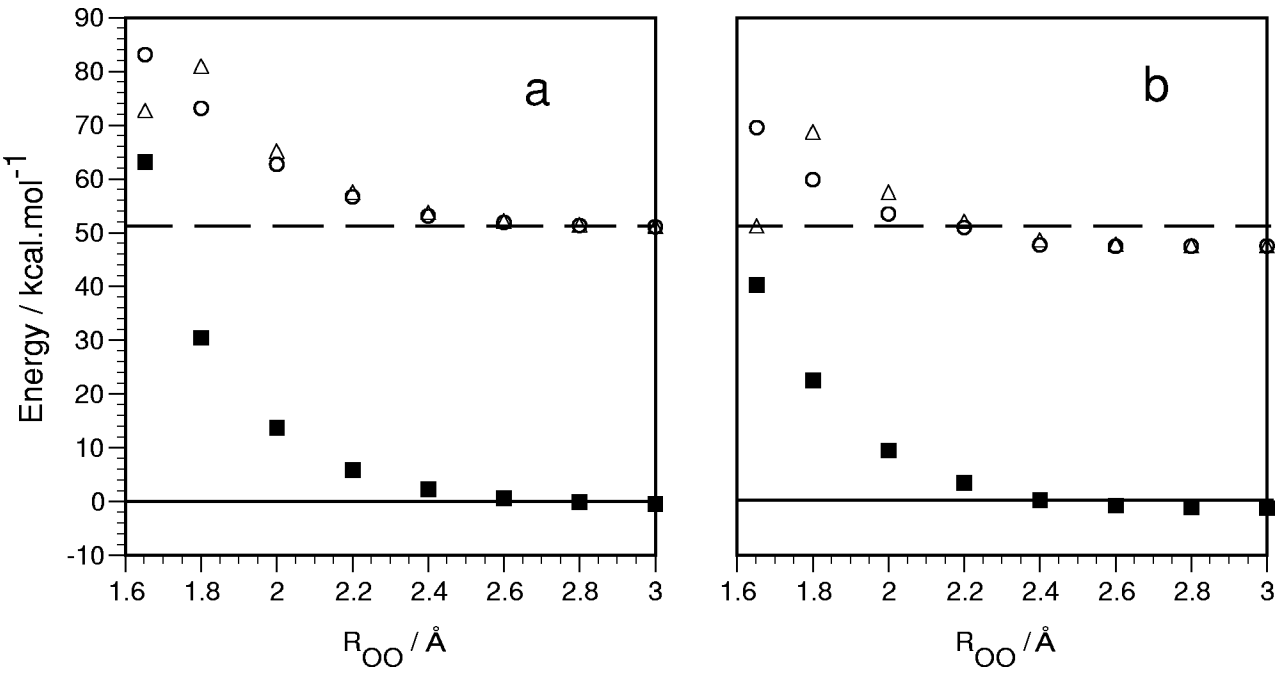

FIG. 4. Energy relative to reactants $[O(^3P)+N_2O]$ for the $^3A''$, $^1A''$, and $^1A'$ PESs, in front of the OO distance [channel (2)], taken as reaction coordinate, with the rest of parameters optimized at the CASSCF(14,12) level for the $^3A''$ state: (a) CASSCF calculations: $^3A''$ ("---■---"), $^1A'$ ("---○---"), $^1A''$ ("---△---"); (b) CASPT2 calculations: $^3A''$ ("—■—"), $^1A'$ ("---○---"), $^1A''$ ("---□---").

geometry is rather different to those found in the MEP of the $^3A''$ PES. Therefore, it seems that a triplet–singlet ISC does not exist at geometries around the MEP.

This negative result led us to explore the alternative that the $^3A''$ PES crossed with the $^3A'$ PES, that does not correlate with ground electronic state products $[N_2(X\,^1\Sigma_g^+)+O_2(X\,^3\Sigma_g^-)]$ but instead with $N_2(X\,^1\Sigma_g^+)+O_2(C\,^3\Delta_u)$. To this aim, we carried out a search of intersection points at the state-average CASSCF level employing the minimum energy crossing point algorithm[41] as implemented in the GAUSSIAN 98 package.[19] For practical reasons the active space had to be reduced to a minimum, i.e., four electrons in three orbitals, which corresponds to the oxygen atom $2p$-derived ones. In these calculations, the Cartesian Pople 6-31G(d) basis set was chosen. With this procedure we obtained the following structure: $R_{NN}=1.08$ Å, $R_{NO}=1.29$ Å, $R_{ON}=1.96$ Å, $<$NNO$=158°$, $<$OON$=148°$, $<$OONN$=180°$. We performed CASPT2 and CASSCF (14,12) pointwise calculations on this structure, obtaining $^3A''-^3A'$ energy gaps of 1.1 and 1.3 kcal mol^{-1}, respectively. Therefore, it can be inferred that the minimal (4,3) active space contains the relevant interactions to account for the surface crossing, so that a good prediction is achieved. The energy of this point relative to reactants for the $^3A''$ state is 32.4 (25.9) kcal mol^{-1} at the CASSCF (CASPT2) (14,12) level. If this point is to act as the effective barrier to reaction, the latter will be lowered by about 14 kcal mol^{-1} with respect to TS A1 (see Table III).

IV. SUMMARY

An *ab initio* study of the $^3A''$ ground PES of the $O(^3P)+N_2O(X\,^1\Sigma^+)$ reaction has been performed at the CASPT2//CASSCF level. The stationary points on the two reactive channels have been characterized. Two paths are found in channel (1), bearing predominant *cis*- and *trans*-arrangements. Channel (2) presents similar structures in the entrance region. Most remarkable is the decrease in energy observed when introducing the dynamical correlation. A TST rate constant calculation was performed, reaching almost quantitative agreement with experiment for channel (1). However, for channel (2) there is a great discrepancy with experiment. The location of an ISC, that would reduce the energy barrier in this channel, was not feasible. Nevertheless, a $^3A''-^3A'$ intersection point placed 25.9 kcal mol^{-1} above reactants was located. We suggest this to be a possible lower-energy pathway to products, that could lead to a better accordance with the experiment in what respects to the N_2+O_2 formation.

ACKNOWLEDGMENTS

This work has been supported by the Spanish Ministry of Education and Culture (MEC) through the project DGES PB98-1209-C02-01. Financial support from the "Generalitat de Calalunya" (Autonomous Government of Catalonia), refs. 1998SGR 00008 and 2000SGR 00016, is also acknowledged. R.V. thanks also the "Generalitat de Calalunya" for a "Beca de Formació d'Investigadors" predoctoral research grant. The authors are also grateful to the "Center de Supercomputació i Comunicacions de Catalunya (C^4-CESCA/CEPBA)" for computer time made available.

[1] N. E. Meagher and W. R. Anderson, J. Phys. Chem. A **104**, 6013 (2000), and references therein.
[2] A. Fontjin, A. Goumri, A. Fernández, W. R. Anderson, and N. E. Meagher, J. Phys. Chem. A **104**, 6003 (2000).
[3] B. O. Roos, The complete active space self-consistent field method and its applications in electronic structure calculations, in *Advances in Chemical*

Physics; Ab Initio Methods in Quantum Chemistry II, edited by K. P. Lawley (Wiley, Chichester, UK, 1987), p. 399.
[4] K. Andersson, P.-A. Malmqvist, B. O. Roos, A. J. Sadlej, and K. Wolinski, J. Phys. Chem. **94**, 5483 (1990).
[5] K. Andersson, P.-A. Malmqvist, and B. O. Roos, J. Chem. Phys. **96**, 1218 (1992).
[6] K. Andersson and B. O. Roos, Int. J. Quantum Chem. **45**, 591 (1993).
[7] B. O. Roos, K. Andersson, M. P. Fülscher, P.-A. Malmqvist, L. Serrano-Andrés, K. Pierloot, and M. Merchán, Multiconfigurational perturbation theory—applications in electronic spectroscopy, in *Advances in Chemical Physics: New Methods in Computational Quantum Mechanics*, edited by S. A. Rice (Wiley, New York, 1996), p. 219.
[8] P. Pulay and T. P. Hamilton, J. Chem. Phys. **88**, 4926 (1988).
[9] J. M. Anglada and J. M. Bofill, Chem. Phys. Lett. **243**, 151 (1995).
[10] K. Wolinski and P. Pulay, J. Chem. Phys. **90**, 3647 (1989).
[11] SURVIBTM, W. C. Ermler, H. C. Hsieh, and L. B. Harding, Comput. Phys. Commun. **51**, 257 (1988).
[12] P. C. Hariharan and J. A. Pople, Theor. Chim. Acta **28**, 213 (1973).
[13] R. Krishnan, J. S. Binkley, R. Seeger, and J. A. Pople, J. Chem. Phys. **72**, 650 (1980).
[14] M. J. Frisch, J. A. Pople, and J. S. Binkley, J. Chem. Phys. **80**, 3265 (1984).
[15] M. González, R. Valero, and R. Sayós, J. Chem. Phys. **113**, 10983 (2000).
[16] R. Sayós, R. Valero, J. M. Anglada, and M. González, J. Chem. Phys. **112**, 6608 (2000).
[17] K. Andersson, Theor. Chim. Acta **91**, 31 (1995).
[18] K. Andersson, M. R. A. Blomberg, M. P. Fülscher *et al.*, MOLCAS, Version 4.1, Lund University, Sweden, 1998.
[19] M. J. Frisch, G. W. Trucks, H. B. Schlegel *et al.*, GAUSSIAN 98, Revision A.7, Gaussian, Inc., Pittsburgh, PA, 1998.
[20] J. L. Teffo and A. Chédin, J. Mol. Spectrosc. **135**, 389 (1989).
[21] K. P. Huber and G. Herzberg, *Molecular Spectra and Molecular Structure, Vol. IV. Constants of Diatomic Molecules* (Van Nostrand Reinhold, New York, 1979).
[22] H. Okabe, *Photochemistry of Small Molecules* (Wiley, New York, 1978).
[23] S. Bashkin and J. O. Stoner, Jr., *Atomic Energy Levels and Grotrian Diagrams* (North-Holland, Amsterdam, 1975), Vol. I.
[24] C. W. Bauschlicher, Jr. and S. R. Langhoff, J. Chem. Phys. **89**, 4246 (1988).
[25] R. Broer and W. C. Nieuwpoort, J. Mol. Struct.: THEOCHEM **458**, 19 (1999), and references therein.
[26] R. Seeger and J. A. Pople, J. Chem. Phys. **66**, 3045 (1977).
[27] A. Sanchez de Meras, M.-B. Lepetit, and J.-P. Malrieu, Chem. Phys. Lett. **172**, 163 (1990).
[28] N. Ghihery, J.-P. Malrieu, D. Maynau, and K. Handrick, Int. J. Quantum Chem. **61**, 45 (1997).
[29] A. Zaitsevskii and J.-P. Malrieu, Chem. Phys. Lett. **228**, 458 (1994).
[30] A. D. McLean, B. H. Lengsfield III, J. Pacansky, and Y. Ellinger, J. Chem. Phys. **83**, 3567 (1985).
[31] C. P. Blahous III, B. F. Yates, Y. Xie, and H. F. Schaeffer III, J. Chem. Phys. **93**, 8105 (1990).
[32] L. Engelbrecht and B. Liu, J. Chem. Phys. **78**, 3097 (1983).
[33] E. R. Davidson and W. T. Borden, J. Phys. Chem. **87**, 4783 (1983).
[34] P.-A. Malmqvist, Int. J. Quantum Chem. **30**, 479 (1986).
[35] P.-A. Malmqvist and B. O. Roos, Chem. Phys. Lett. **155**, 189 (1989).
[36] M. Merchán, R. Pou-Amérigo, and B. O. Roos, Chem. Phys. Lett. **252**, 405 (1996).
[37] L. Rodríguez-Monge and S. Larsson, Int. J. Quantum Chem. **61**, 847 (1997).
[38] D. G. Truhlar, A. D. Isaacson, and B. C. Garrett, in *Theory of Chemical Reaction Dynamics*, edited by M. Baer (CRC, Boca Raton, FL, 1985), Vol. 4, p. 65.
[39] J. I. Steinfeld, J. S. Francisco, and W. L. Hase, *Chemical Kinetics and Dynamics* (Prentice-Hall, Englewood Cliffs, NJ, 1993), p. 318.
[40] D. R. Yarkony, Electronic structure aspects of nonadiabatic processes in polyatomic systems, in *Modern Electronic Structure Theory, Part I*, edited by D. R. Yarkony (World Scientific, Singapore, 1995).
[41] M. A. Bearpark, M. A. Robb, and H. B. Schlegel, Chem. Phys. Lett. **223**, 269 (1994).